Sub-nanosecond resolution x-ray magnetic circular dichroism photoemission electron microscopy of magnetization processes in a permalloy ring

2005 J. Phys.: Condens. Matter 17 S1381

(http://iopscience.iop.org/0953-8984/17/16/009)

INSTITUTE OF PHYSICS PUBLISHING JOURNAL OF PHYSICS: CONDENSED MATTER

J. Phys.: Condens. Matter **17** (2005) S1381–S1395 doi:10.1088/0953-8984/17/16/009

Sub-nanosecond resolution x-ray magnetic circular dichroism photoemission electron microscopy of magnetization processes in a permalloy ring

D Neeb[1], A Krasyuk[1], A Oelsner[1], S A Nepijko[1], H J Elmers[1], A Kuksov[2], C M Schneider[2] and G Schönhense[1,3]

[1] Institut für Physik, Johannes Gutenberg-Universität Mainz, D-55099 Mainz, Germany
[2] Institut für Festkörperforschung IFF-6, Forschungszentrum Jülich, D-52425 Jülich, Germany
[3] GST mbH, Alexander Fleming Straße 65, D 55130 Mainz, Germany

Received 1 November 2004
Published 8 April 2005
Online at stacks.iop.org/JPhysCM/17/S1381

Abstract

Fast magnetization processes in a microstructured permalloy ring with 80 μm o.d. and 30 nm thickness have been observed by photoemission electron microscopy exploiting x-ray magnetic circular dichroism as the magnetic contrast mechanism. As a high speed probe we employed synchrotron radiation pulses at the ESRF (Grenoble) operated in 16-bunch mode, yielding photon pulses of 105 ps FWHM with a period of 176 ns. Fast magnetic field pulses have been generated by means of current pulses through coplanar waveguides with the magnetic structure being lithographically prepared on their surface. A stroboscopic pump–probe set-up with a variable time delay between the field pulse and photon pulse allowed us to take snapshots of the dynamic response of the magnetic domain structure. We observed coherent magnetization rotation during the leading edge part of the field pulse, the formation of a characteristic domain pattern ('onion state') in the plateau region of the pulse and the fast formation of a striped domain pattern (incoherent magnetization rotation) during the trailing edge part of the field pulse. A numerical simulation confirmed essential features of the stroboscopic image series.

1. Introduction

The need for methods for exploring and controlling the fast dynamic response of magnetic thin film elements in the sub-nanosecond regime has become more and more urgent and interesting over the last decade. It is not only driven by the desire for a more thorough understanding of physics in that regime, but is paramount for industrial applications, e.g. in the development of new magnetic storage devices, such as hard disks with a greater storage density or magnetic RAM and spintronics elements. A prerequisite for controlling the dynamic behaviour of the

magnetization is a thorough characterization and understanding of the magnetic responses with appropriate lateral and temporal resolutions. When the dynamic behaviour comes into play, high storage densities are inevitably correlated with fast data transfer rates and therefore short switching times of the order of a few nanoseconds down to below one nanosecond.

The majority of methods for magnetic imaging with high lateral resolution work on the basis of scanning probe techniques. The sequential scanning of lines along the sample surface prevents a high temporal resolution. There are optical methods for achieving the desired temporal resolution such as magneto-optical Kerr microscopy [1], but the lateral resolution is limited by the diffraction of light and therefore not sufficient for investigating devices with critical dimensions of the order of 100 nm.

These considerations motivated us to use a parallel imaging technique with high lateral resolution such as photoemission electron microscopy (PEEM). A stroboscopic pump–probe set-up with variable delay time allows us to take snapshots of the domain dynamics. The concept for static domain imaging on the basis of x-ray magnetic circular dichroism (XMCD) has been discussed in various publications (see [2, 3] and references therein). Fast magnetic field pulses are applied employing coplanar waveguides with the magnetic structures being deposited on the surface of the waveguide. The instrument used for the experiments described in this paper was a modified commercial instrument [4]. Apart from the possibility of a precise adjustment of the sample prior to the experiment *ex situ* and piezomotor-driven sample positioning, the advantage of the integrated sample stage is the elimination of relative movement of the stage and microscope because of vibrations and/or drift. This ensures long measurement series with exactly reproducible lateral positions. A sample holder with high frequency compatible plugs allows *in situ* exchange of the magnetic sample and the waveguide. The parallel imaging mode permits the observation of the whole field of view (typically a few microns up to a few 100 μm) at the same time by a stroboscopic procedure, necessary for sufficient image intensity. This approach relies on a strictly periodic remagnetization process. The validity of this assumption will be discussed. First time-resolved measurements using stroboscopic imaging with synchrotron radiation in the soft x-ray range in combination with PEEM have been demonstrated by Krasyuk *et al* [5], Vogel *et al* [6] and later Choe *et al* [7].

In this paper we present results obtained with a considerably improved set-up and discuss the characteristics of the stroboscopic technique. An *in situ* detection method for the transient field pulse has been developed and utilized for a precise correlation of the domain snapshots with the temporal profile of the magnetic field pulse. Results for a thin, lithographically prepared permalloy ($Ni_{80}Fe_{20}$) ring reveal several processes with sub-nanosecond dynamics.

2. Experimental set-up

2.1. A coplanar waveguide on an exchangeable sample holder

The sample was fabricated in a multi-step process. First, a 100–250 nm thick Cu coplanar waveguide (microstripline) was prepared on a SiO_x/Si substrate (thermally oxidized Si wafer) via photolithography and wet chemical etching. For this purpose, two insulating paths have been cut out of a homogeneous Cu film for creating the stripline. Beyond the insulating gap on both sides of the stripline there is a homogeneous Cu film as the ground shield. This fact is important for bandwidth aspects: the whole set-up is designed to achieve 50 Ω impedance, when the Cu layer adjacent to the waveguide is grounded. A photograph of the 100 μm wide waveguide carrying magnetic microstructures of various shapes is shown in figure 1(a). The magnetic microstructures were produced by depositing permalloy (Py) on the stripline by means of DC magnetron sputtering and subsequent ion milling for achieving the desired

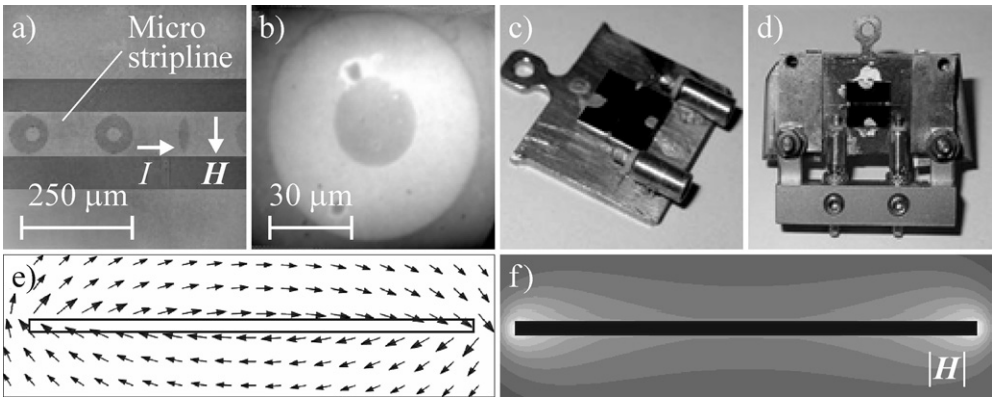

Figure 1. An optical image of the coplanar waveguide carrying various permalloy microstructures (a) and a PEEM image of a Py ring (b) microstructured on the waveguide surface. The device is mounted on an exchangeable sample holder (c) that can be inserted with MMCX microwave plugs into a carrier frame (d). A cross section of the microstripline with the magnetic field distribution $\boldsymbol{H}(r)$ and a contour plot of $|H(r)|$ are depicted in (e) and (f), respectively.

geometry. Finally, a protecting layer of 2 nm of Cu was deposited, which was removed *in situ* prior to the XMCD–PEEM measurements via mild ion bombardment.

Figure 1(b) shows a PEEM image of one of the Py structures, the ring visible in the centre of figure 1(a). We will discuss the static and dynamic domain images of this ring structure (outer diameter 80 μm, inner diameter 32 μm, thickness 30 nm) in section 4. Figures 1(c) and (d) show the exchangeable sample holder. In order to apply magnetic field pulses inducing remagnetization processes in the Py microstructures a fast current pulse was fed through the waveguide. The sample stage is equipped with an electric docking station, which is realized by two MMCX plugs[4]. The MMCX standard is one of the smallest industrially manufactured microwave systems and these plugs, in particular, are specified for bandwidths of up to 6 GHz by the producer. The corresponding sockets are located at the sample holder, where the connection is made to the coplanar waveguide via short thin Cu wires.

The electrical pulse was delivered by a pulse generator[5] with an external trigger. The rise time of the voltage pulse was 800 ps and its FWHM about 7.5 ns. According to the law of Biot and Savart, a magnetic field (Oerstedt field) is induced by the current through a conductor. The strength of the corresponding magnetic field is approximately 2 mT. The field distribution is sketched in figures 1(e) and (f). Interestingly, the extrema appear close to the rims of the stripline due to the occurrence of an additional out-of-plane component. The parallel component stays almost constant.

2.2. Stroboscopic XMCD–PEEM using synchrotron radiation

A schematic view of the experiment for stroboscopic imaging of the field pulse induced variation of the ferromagnetic domain structures is shown in figure 2. Here, the light source was the European Synchrotron Radiation Facility (ESRF) in Grenoble. In the 16-bunch mode used, the photon pulses have a maximum FWHM of 105 ps and a repetition period (time distance) of 176 ns. 'Snapshots' have been taken in the stroboscopic mode by synchronizing the current pulse along the waveguide with the photon pulses. A trigger signal from the storage ring (bunch marker) is delayed with an adjustable component, before starting the field pulse.

[4] Amphenol, MMCX type.
[5] Ultrafast pulse generator, Kentech type (UK).

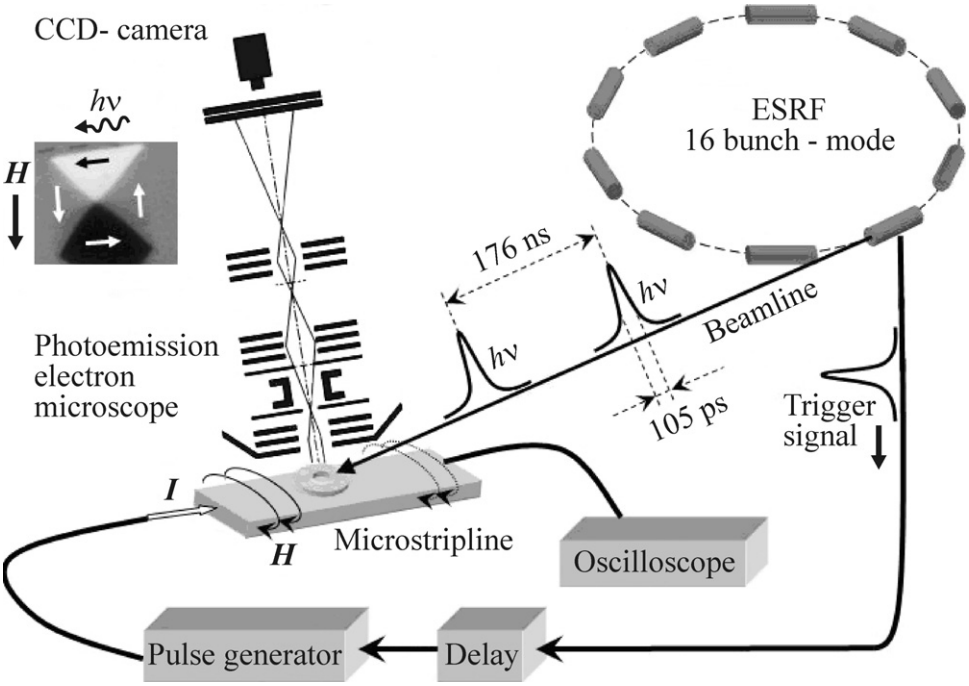

Figure 2. The set-up for stroboscopic imaging of the field pulse induced magnetization dynamics of ferromagnetic structures. The experiment employed x-ray magnetic circular dichroism as the contrast method. It was performed at the ESRF (Grenoble). Inset: the scheme for the geometry yielding the XMCD contrast.

Through stepwise adjustment of the delay in 500 ps steps the field pulse is moved with respect to the photon pulse. In the present experiment the total time resolution defined by photon pulse width and electronic jitter (about 60 ps) is approximately 125 ps. This value could be reduced very recently by about one order of magnitude [8] in the special low alpha mode at Berlin Electron Storage Ring for Synchrotron Radiation (BESSY II) [9, 10]. Thus the magnetic domain structure can be imaged at different delay times between excitation and probing. At the photon intensities delivered by third-generation storage rings it is impossible to acquire an image within a single photon pulse. In a typical exposure time of 120 s at a given delay setting, the image averages over about 7×10^8 cycles in the stroboscopic mode.

A photon energy of $h\nu = 853$ eV corresponding to the Ni L_3 edge was chosen for observing the domains in the Py structures of the sample. The L_3 absorption edge is a strong 'white line' and Ni is the main constituent of Py ($Ni_{80}Fe_{20}$). For details on the PEEM technique and on the relevant contrast mechanisms (magnetic and other), see [3]. The angle of the photon beam with respect to the surface normal was 65° and its projection onto the sample surface was parallel to the microstripline; see figure 2. This geometry yields a contrast of the domains with their magnetization *perpendicular* to the external field $\boldsymbol{H}$; see the inset in figure 2. We will see below that this geometry is advantageous for the present study.

3. Special features of XMCD–PEEM using magnetic samples on microstriplines

3.1. The influence of the pulsed microstripline on the image quality

A crucial question at the beginning of the field pulsed experiments was, to what extent the stroboscopic imaging using the microstripline technique degrades the resolution and contrast

or causes artefacts. Initially, we checked whether *charging of the insulator* besides the stripline influences the image. First PEEM images of a stripline sample with magnetic dots revealed that the dots directly on the stripline and in electrical contact with the stripline appear in focus. Only those magnetic dots on the insulating part of the substrate are blurred due to charging.

A second important issue was the *action of the Lorentz force on the electron trajectories* during the magnetic field pulse application. As the electrons have low starting energies of up to a few electronvolts only, the influence of the Lorentz force is often regarded as spoiling the image quality completely. At least, it can be expected to be visible in the images. We studied this phenomenon for cobalt squares on a microstripline. Indeed, the Lorentz force caused a visible deformation of the images of the magnetic structures. In the survey mode of the microscope the outer edges of the structures appear shifted by distances of the order of 1 μm, with the direction of the shift clearly depending on the local field direction. Upon reversal of the direction of the current pulse the direction of the image shift is also reversed. In the field free state the structure appears without deformation. Despite this image deformation the edge itself appears always sharp, i.e. the lateral resolution is not diminished. As the image deformation can be analytically calculated, it can be exploited as a measure for the corresponding local magnetic field strength [11]. This shift provides a tool for determining the temporal profile of the field pulse from the image deformation [5]. This technique of imaging the effect of the Lorentz force yields further information on the transient stray fields of the domains [12]. For the thin Py microstructures discussed below, the effect of the Lorentz force is only very weak. The extension of the magnetic stray field into vacuum above the sample scales with the thickness of the magnetic structure (more precisely, with the total flux emerging at the corners of the structure). Thus the integral action of the Lorentz force upon the low energy electrons also scales with the sample thickness at a given value of sample magnetization.

There is a third phenomenon besides charging and Lorentz force that is of importance for the image interpretation. The current pulse generating the magnetic field is connected with a corresponding *voltage pulse travelling along the coplanar waveguide*. In cathode lens microscopes the sample surface is an active part of the objective lens. Hence, the voltage pulse, i.e. a transient potential change, influences directly the electron optical properties. Besides image focusing, the lateral magnification is also influenced at certain parameter sets of the electron optics. This leads to the effect of 'chromatic aberration of magnification' [13] being very useful for the stroboscopic imaging technique, as will be demonstrated in the next section.

3.2. Determination of the field pulse profile via the image magnification

The results displayed in figure 3 illustrate the effect of the voltage pulse running along the waveguide. Two PEEM images at identical microscope settings but different time delays are shown in the top left panels. Obviously, the image size of the Py ring changes with time. At the given settings the voltage pulse causes an enhancement of the magnification factor by 14% ('breathing' of the image) along with a small deviation from the ideal focus position. This temporal variation of the magnification factor as visible in the series of image stripes in the top right panel can be evaluated and provides a measure for the temporal profile of the local field strength. At the bottom panel of figure 3 the *in situ* temporal pulse profile extracted from the magnification factor is shown as circles. The full lines shown for comparison represent the electrical pulse profiles measured directly at the pulse generator output (full) and at the exit point of the electrical RF lines from the UHV chamber (dotted). These curves have been measured using a fast oscilloscope. At the exit the shape resembles the loading curve of a capacitor, which is caused by the capacitance of the stripline and cables. As could be expected, the *in situ* rise time lies between the electrically measured profiles at the input and output of the

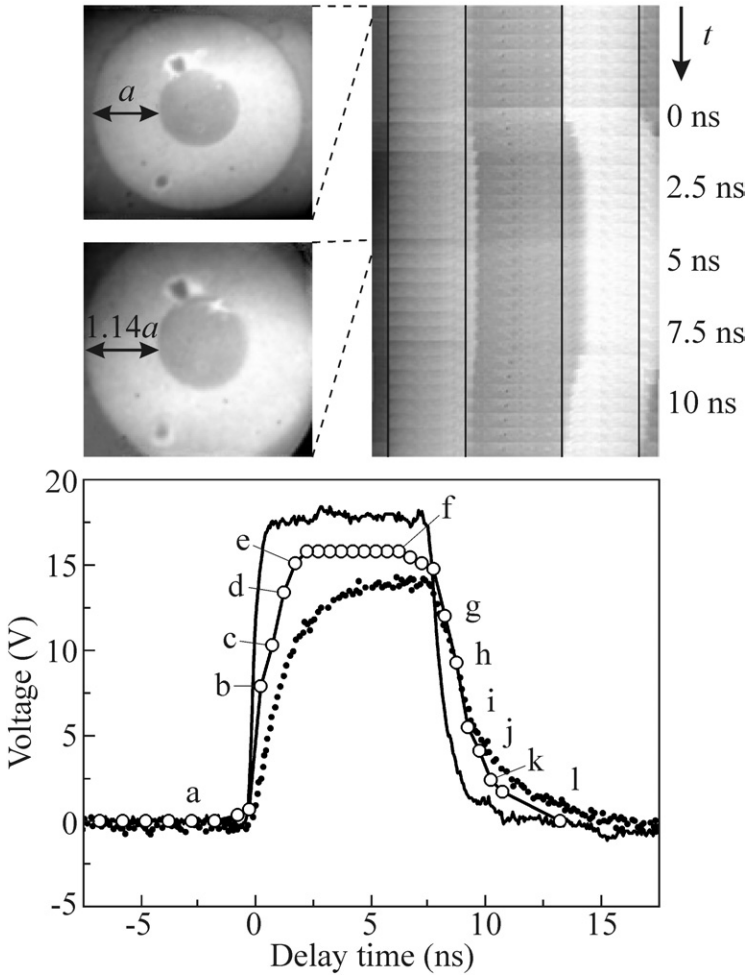

Figure 3. The action of the voltage pulse travelling along the waveguide on the image magnification of the microscope optics exploited as an internal probe of the pulse profile. Top left: images taken at times before the pulse onset and in the pulse plateau, respectively, revealing an increase of the image magnification during the time of presence of the voltage pulse. Top right: the sequence of stripes across images taken with 500 ps time increments. Note the transient change of magnification in the pulse regime. Bottom: the resulting temporal pulse profile as measured *in situ* (circles) in comparison with the pulse profiles measured at the entrance and exit of the RF lines into the UHV chamber (full and dotted, respectively). Points (a)–(l) correspond to the image series in figure 5.

electrical set-up. As the electrical leads on the two sides of the stripline are identical we have drawn the maximum halfway between the two oscilloscope curves. The estimated relative errors are about the size of the circles.

The rise time of the effective field at the sample is 1.8 ns, i.e. about two times larger than the rise time of the pulse generator output. The slope in the steepest part of the leading edge is about 1 mT/500 ps. The following plateau is maintained for about 5 ns, before the drop with a maximum slope of approximately 0.5 mT/500 ps sets in. The whole image distortion takes place in roughly 10 ns, after which the original image size is restored again; see the top right panel. This is about 2.5 ns longer than the pulse duration at the pulser output. The broadening

is almost identical at the leading and trailing edges. The initial part of the leading edge is almost as fast as the pulser output.

In these experiments it turned out that the magnification factor is extremely helpful information for precisely locating the leading and trailing edges of the field pulse on the sub-ns timescale. On the other hand, this factor can be easily eliminated for an evaluation of the magnetization dynamics by rescaling all partial images to the same size. Proper focusing of all individual images is, of course, possible. If undesired, the effect can be largely suppressed when the microscope optics is operated at minimum refractive power of the objective lens.

4. Magnetic contrast of the permalloy ring

4.1. Static domain pattern

For imaging the magnetic domain structure, XMCD asymmetry images for excitation with light of right- and left-handed helicity have been measured as described, e.g., in [3]. In these images all contrast contributions other than magnetic are cancelled. The XMCD asymmetry scales with the scalar product of the local magnetization $\boldsymbol{M}$ and photon helicity. Thus, the grey value in the asymmetry image gives, in principle, direct access to the direction of the local magnetization vector (except for the ambiguity of the cosine function). In practice, the intensity of the synchrotron radiation drops continuously during image acquisition. Consequently the second image (taken with reversed helicity) has to be scaled by an empirical factor in order to achieve identical brightness scales. This scaling can be a source of systematic error. In addition, inhomogeneous illumination can cause further artefacts, in particular when it changes between the two helicities. We estimate the total error to be about $\pm 8\%$ of the absolute asymmetry values.

Figure 4 shows a static asymmetry image of the Py ring taken without external field pulse excitation. The shape of the ring appeared somewhat distorted due to electron optical artefacts (image field distortion). This effect has been eliminated by image processing in figures 4 and 5. The stripline had been pulsed before, so the observed magnetic pattern is not a ground state, but represents a metastable configuration after domain movement. Nonetheless, this pattern was stable for several hours; a similar observation was found for diamond-shaped Py structures, staying for hours in a metastable '*s*-state' [14]. Measurements of similar Py ring structures with smaller dimensions have shown a continuous magnetization rotation (vortex state) [15]. This is obviously not the case here, which is most likely the result of prior switching along with the larger size of the structure.

To examine the possibility of still existing regions with continuous magnetization rotation, a circular line scan of the XMCD asymmetry has been carried out; see the bottom panel. Clearly, the structure still has a 'memory' of the vortex state. The correlation of the measured asymmetry in region A (between 40° and 160°) with a cosine function is obvious. A comparable behaviour occurs in domain B (225°–290°). Apart from these remnants of a stray field free configuration, pronounced domain structures are present, which resemble our findings for exchange-biased structures [15].

One particularly interesting magnetization pattern (C–F) known from rectangular Py structures is found at the left-hand side of the ring. It is very similar to a Landau-type flux closure configuration, with the domain magnetization orientation being indicated by the arrows. Even though the orientation of the magnetic domains in comparison to the rectangular case is slightly distorted, it is surprisingly close to a structure with 90° walls only. While the upper and lower domain (C and D) nearly approach the ideal case, the left and right (E and F) domain show rotation asymmetry. This is quite understandable, because of the outer perimeter of the

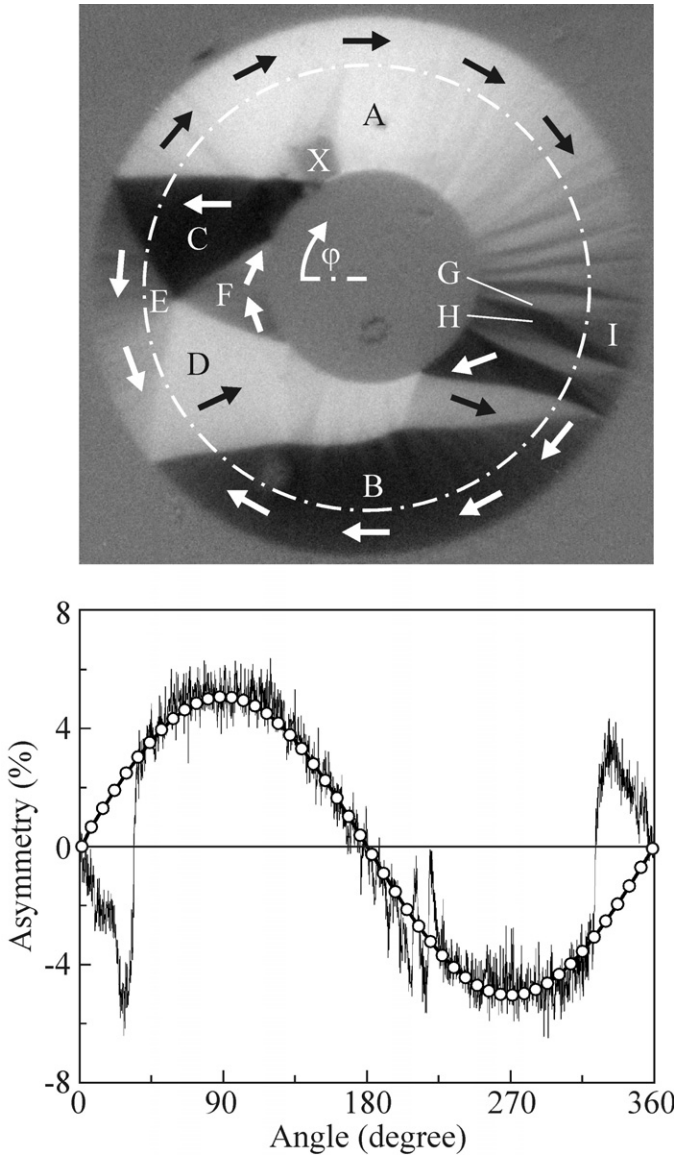

Figure 4. Top: a static domain image of the field free state of a permalloy ring (o.d. 80 μm, i.d. 32 μm, thickness 30 nm). The magnetic contrast is due to XMCD at the Ni L_3 edge ($h\nu = 853$ eV). The photon impact direction points from left to right. The local magnetization directions are denoted by arrows. Bottom: an intensity line scan along the circumference (chain circle in top image) quantifying the domain structure in the field free case. The dotted curve is a fit to region A and denotes the behaviour expected for a continuous rotation of the magnetization (vortex state).

domains: the left and right areas are limited by the curved borders of the ring while the wall positions of the upper and lower domain are set by interaction with neighbouring domains. A reason for the nearly horizontal upper wall of domain C, and the resulting close resemblance to the rectangular case, most likely is connected with the position of the pinning defect in the Py

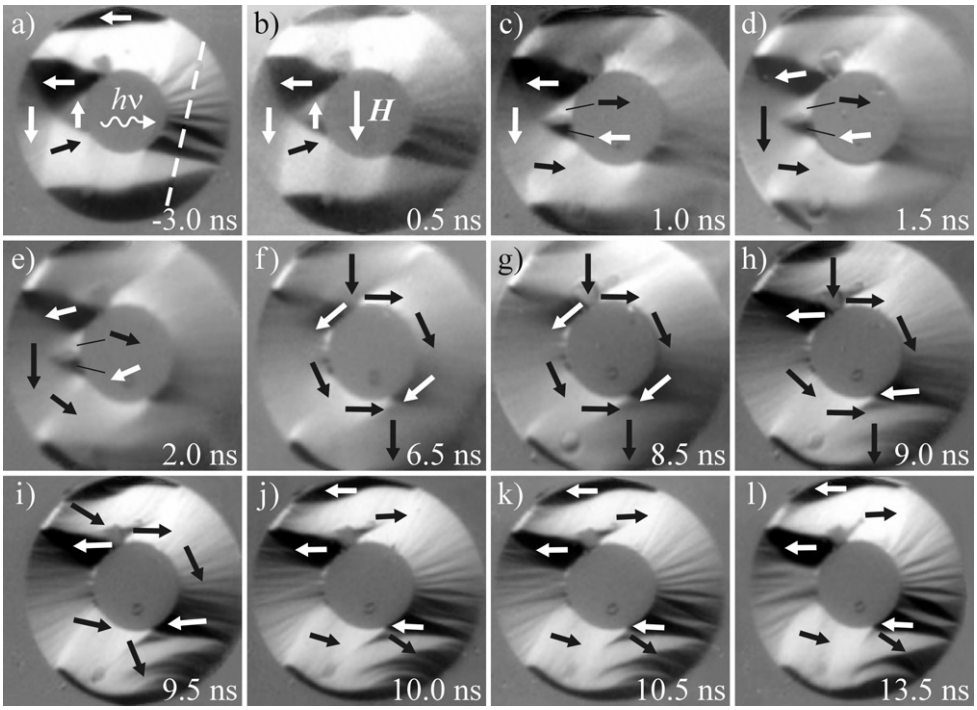

Figure 5. Dynamic behaviour of the domain pattern of a permalloy ring (o.d. 80 μm, i.d. 32 μm, thickness 30 nm). (a)–(l): stroboscopic image series (snapshots) of the temporal variation of the pattern at different time delays as marked in figure 3, bottom panel. The numbers denote the time with respect to the pulse onset; the arrows indicate the local magnetization direction. Magnetic contrast is due to XMCD at the Ni L_3 edge ($h\nu = 853$ eV).

structure (the defect marked by X). Domains C–F form a vortex feature; the fact that this special feature occurs in a ring structure has also been found in micromagnetic simulations [16, 17].

Another interesting system of domains is the structure on the right-hand side of the ring. This pattern consists of alternating darker and lighter domains pointing outward or inward, respectively. The oscillatory behaviour shows up most obviously in the bottom part of figure 4 (angle 160°–225°) and is possibly driven by anisotropy to locally close the fluxes and therefore minimize the stray field. On closer inspection, one can find a partition of the spikes into groups giving rise to another flux closure induced pattern. It seems that parts of the spikes form a flux closure out of three domains as in G–H–I. Yet, because of the direction of the walls we conclude that the walls are not 90° walls. Minimization of stray fields at the rim leads to the formation of closure domains at the outer and inner rim of the ring with magnetization components tangential to the perimeter. Dark and bright domains with magnetization components perpendicular to the perimeter become narrow at the inner and outer rim. The domain wall of B reveals weakly pronounced cross-tie wall features, characteristic of 180° walls for Py in this thickness range.

4.2. Dynamic behaviour

The asymmetry images corresponding to different delay times are shown in figures 5(a)–(l). The corresponding times are given with respect to the onset of the field pulse as denoted in the pulse profile; figure 3. The similarity of the image taken before the pulse onset (a) and the field free case (figure 4) is evident. There are some differences, in particular the dark domain on

top and the size of the dark domain at the bottom, which indicate that the magnetic structure did not fully relax. Another difference is found in the flux closure pattern (C–F). The left domain (E) with a magnetization direction parallel to the induced field is still larger than in the field free case (figure 4) while domain F with antiparallel magnetization orientation is still smaller in size. Since in figure 5(a) the exciting pulse had not reached the field of view yet, it is easy to assume that the differences in the magnetic structures are derived from the prior excitation in the stroboscopic measurement. Obviously the system did not have time to relax completely during the time of 176 ns between two exciting pulses. As mentioned above, the domain pattern of figure 4 is also metastable and does not reflect the lowest energy state which would be a vortex state.

At the onset of the field pulse the overall domain structure remains stable while the maximum asymmetry contrast decreases, indicating that the external field causes mainly a coherent magnetization rotation within domains that were magnetized perpendicular to the field pulse. This effect can be seen most prominently at the flux closure structure (C–F). The original shape of domain F can be identified even until the maximum field is reached in figure 5(e). Although the asymmetry decreases at the onset of the field pulse, in most areas there exist noticeable deviations from a homogeneous magnetization rotation. Before the field pulse has arrived the magnetization is antiparallel to the external field direction in domain F. With increasing field the magnetization rotates clockwise in the upper and anticlockwise in the lower part of domain F, leading to a pair of almost antiparallel magnetized domains within the original area of this domain. A second striking feature is observed at the points where domains C and D touch the outer rim of the ring, where narrow domains with magnetization direction perpendicular to the field are formed.

The vortex position of the flux closure structure (C–F) remains stable at the initial onset of the field pulse. The magnetization rotates during this time in domains C and D exclusively in a distinct area close to the initial 90° walls between C and E as well as D and E. Thus domain E has effectively expanded. In figure 5(c) the initial position of the 90° wall between C and E as observed in figures 5(a) and (b) and the new boundary as identified in figure 5(d) can both be observed. Unfortunately, no data are available in between these two snapshots. If the domain wall moved continuously the movement had to have happened considerably faster than the temporal resolution of about 100 ps. As a consequence the domain wall speed had to exceed 10^4 m s^{-1} which would be in contrast to current experimental and theoretical results [18, 19]. Instead of a continuous domain wall movement, a coherent magnetization rotation has occurred. Taking into account the material parameters of permalloy a magnetization rotation of 90° may well take place on such a short timescale. This observation is clearly dominated by the dynamical behaviour of the magnetization reversal. Instead, for a quasistatic reversal one would expect a continuous shift of the vortex of the flux closure structure (C–F) with increasing external field.

During the plateau part of the field pulse (figures 5(e)–(f)) the initial vortex of the flux closure structure C–F continuously moves towards the inner rim leaving narrow regions of horizontal magnetization at the inner rim of the ring. As in domain F in most parts of the ring the asymmetry has vanished indicating that the magnetization points essentially homogeneously along the external field. Exceptions occur only at the inner and outer rim of the ring. The prominent magnetization distribution resembles an onion state [16, 17] as indicated in figure 5(f). In this special configuration the magnetic flux that has entered the ring from the top is led to the left and right side of the ring at the inner hole. The magnetic flux then joins again at the lower part of the inner ring and finally leaves the ring at the bottom. The axis of the onion state is inclined with respect to the direction of the external field. This may be caused by the structural defect X (see figure 4).

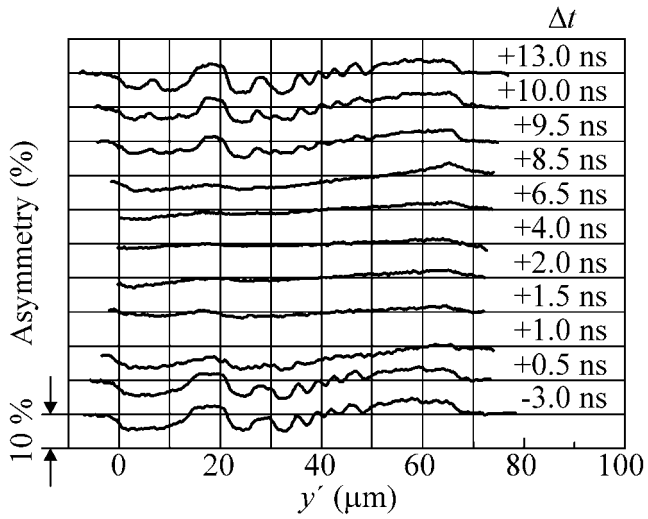

Figure 6. Intensity line scans along the dashed line in figure 5(a) for different delay times after the onset of the field pulse. The length scale y' was normalized in order to correct for the variation of magnification and for the lateral shift when the field pulse passes the field of view. The bottom and top rim positions are at 0 and 67 μm, respectively.

The stroboscopic character of the measurement is responsible for the fact that only periodic domain and wall movements can be seen. Therefore the apparently grey areas in figures 5(e)–(g) could possibly hide a random movement of domains. However, if one takes the temporal development into account, the case of a largely downward orientation, as indicated by the arrows in figure 5(f), is much more likely.

Particularly interesting is the image sequence along the trailing edge. Starting in figure 5(g) but more clearly in figures 5(h)–(l) the whole ring structure is penetrated by a fine ripple pattern, most clearly visible in the line scans; see figure 6. At the end of the field pulse figure 5(l) the fine stripes partly unify leading to a coarser 'blocking' pattern. It seems obvious that this pattern is relatively stable and thus needs time to decay back into the Landau pattern at the foot of the leading edge of the next field pulse, 176 ns later. Furthermore, it is evident that the flux closure structure (C–F) has not formed yet behind the trailing edge of the pulse (figure 5(l)) although the external field is zero. Here, the remagnetization is driven by the demagnetizing field. In contrast to the coherent magnetization rotation in domains C and D at the leading edge of the pulse, the trailing edge causes an incoherent magnetization change; see [20]. The development of the flux closure structure thus takes considerably more time than its disintegration. The stripe-like domain pattern observed in the region of domain E in figure 5(l) is an intermediate pattern. Although the stray field is minimized by many locally closed flux features, the number of walls and thus the inherent energy stored in these is high. Therefore it is understandable that this complex structure requires a period of several nanoseconds to relax into the pattern found prior to the exciting pulse; figure 5(a). Whether this decay happens spontaneously or continuously cannot be distinguished here because of the lack of data in that time regime. The first way seems more likely, taking into consideration the relative stability of the first and last structures recorded.

In the trailing edge a stripe domain pattern develops on the right-hand part of the ring, too. There, the domain pattern is more pronounced (higher contrast) indicating that the magnetization rotates earlier perpendicular to the external field. At the foot of the trailing

edge the same domain pattern as in the field free case has almost formed. This domain pattern is then stable until the next field pulse arrives. It is even similar to the domain pattern in the field free case (figure 4). The concertina-like pattern certainly costs more energy than a homogeneous magnetization state. We cannot exclude the possibility that an additional in-plane anisotropy is responsible for this behaviour.

Another interesting finding during the trailing edge part is apparent at the bottom region where the magnetic flux of the onion state leaves the ring. Numerous narrow domains starting at the bottom right area of the outer rim of the ring taper off in an arc-like form towards the left side. This phenomenon is not necessarily linked to the particle shape, because it has been found in perpendicular particles also [21, 22].

The line scans through the stripe domain pattern on the right side of the ring reveal the magnetization directions in this region; see figure 6. The asymmetry reflecting the horizontal component of the magnetization vector is expected to increase from the bottom to the top for a homogeneous vortex state as discussed previously. This general behaviour is well shown by all of the scans, while the stripe domain pattern shows up as an additional oscillation. Most strikingly the position of the domain walls remains constant during the field pulse. A movement of a domain wall is clearly not observed on the length scale of figure 5.

In order to understand the observed magnetization dynamics we performed a numerical simulation using a finite-element approximation [23]. Three selected snapshots are displayed in figure 7. Currently, we are not able to model the complete ring. Instead we approximated the flux closure structure (C–F) by a small square element with an edge length of 1 μm. Starting from a Landau domain pattern, the external field pulse of 50 mT forces domain F (being initially antiparallel to the external field) into a pair of antiparallel oriented domains with a magnetization perpendicular to the external field. This is similar to the experimental observation; see figure 4(d). The simulation shows that this pattern originates from the dynamic movement of the magnetization at the initial domain walls of domain F forming strong magnetic poles at the upper and lower right corner of the flux closure structure at the initial stages of the field pulse. The magnetic stray field originating from these poles is added to the external field and causes a torque on the magnetization in domain F, clockwise for the upper half-domain and anticlockwise for the lower half, thus forming a pair of antiparallel domains in the former area of domain F. A similar simulation for a square of the same lateral dimensions but with a thickness of only 3 nm does not show the formation of antiparallel domains in the former domain F, thus confirming the importance of stray fields for the observed dynamics.

After the field pulse has passed, the pair of antiparallel domains extends throughout the whole square (figure 7(c)) and it takes a surprisingly long time (4 ns in our simulation) to restore the original Landau pattern in the field free state. This behaviour originates from the vortices at the right edge that the external field failed to remove. Again this observation resembles our experimental finding of the horizontal stripe domain pattern in the trailing edge; figures 4(i)–(l). One should note that our square particle simulated here is far from a realistic size and thus is not able to quantitatively explain the experimentally observed magnetization dynamics. Nevertheless, we believe that it explains qualitatively the observed behaviour that may appear as a general feature also in other geometries, e.g. [21, 22].

The appearance of arc-shaped domains with a sharp tip-like end in the bottom part of figures 5(h)–(l) is eye-catching. In the same images the domain boundary of the top dark domain attains an *s*-like shape, whereas it is almost straight in (a)–(d). Inspection of figure 3 reveals that the bent features occur in the region of the highest slope of the trailing edge, i.e. the peak value of $\mathrm{d}H/\mathrm{d}t$. According to the Maxwell equation $\mathrm{d}\boldsymbol{H}/\mathrm{d}t = -(\nabla \times \boldsymbol{j})/\mu\sigma$ this sudden drop of the magnetic field gives rise to eddy currents $\boldsymbol{j}$. The eddy currents, in turn, give rise to magnetic fields that are directed such as to delay the sudden field drop. On the planar stripline

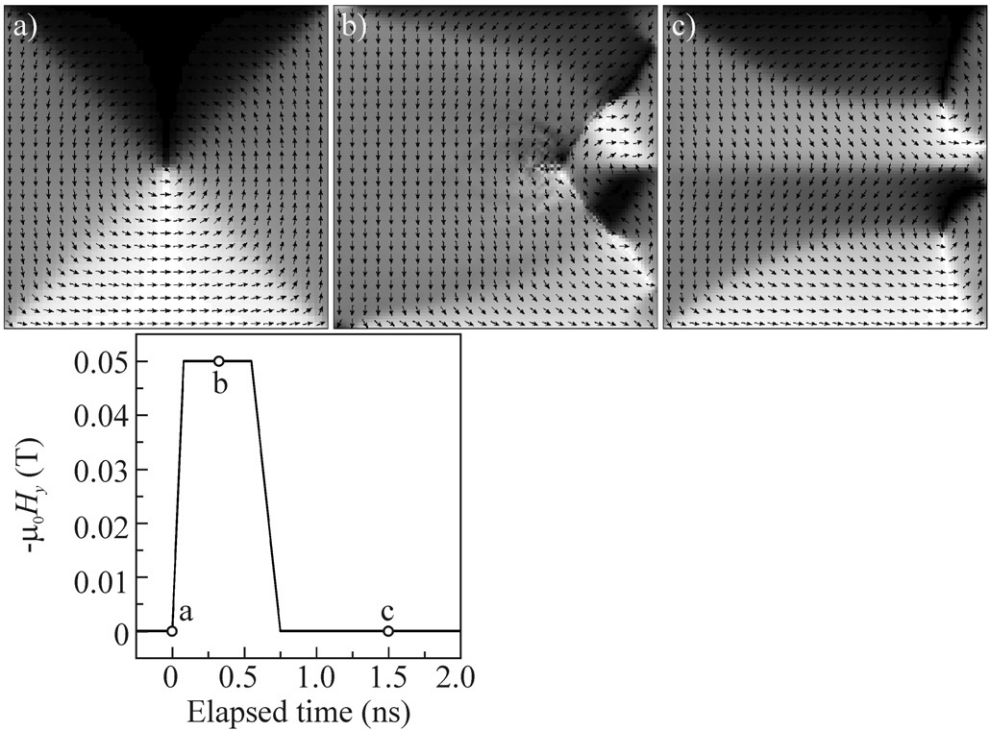

Figure 7. Simulated domain patterns in a square permalloy particle (1 μm × 1 μm) of thickness 20 nm. Snapshots of the time evolution are shown before the field pulse (a), during the field pulse (b) and after the field pulse (c). The calculations were performed using the object oriented micromagnetic framework [23]. The sample was discretized into 100 × 100 × 1 cells and relaxed into its initial state with a damping coefficient of $\alpha = 0.5$. The damping constant was then set to $\alpha = 0.05$ before the pulse was applied with $\boldsymbol{H}$ pointing along the y-axis (from top to bottom).

the eddy currents arise due to the out-of-plane component of $\mathrm{d}\boldsymbol{H}/\mathrm{d}t$. As visible in figure 1(e), this component is maximum at the rims of the stripline, corresponding to the upper and lower rim of the field of view in figure 5, where the bent features occur.

5. Conclusions

A new experimental set-up has been developed that allows stroboscopic PEEM imaging of fast magnetization processes making use of the time structure of synchrotron radiation and x-ray magnetic circular dichroism as the contrast mechanism. Fast magnetic field pulses can be applied by running current pulses through coplanar waveguides mounted on a UHV-exchangeable sample holder. The magnetic structures are prepared by ion beam etching on the surface of the waveguide. The time resolution depends essentially on the photon pulse width. The present results have been taken in the 16-bunch mode of the ESRF (Grenoble) at a FWHM of 105 ps. Very recently, experiments in the low alpha mode of BESSY II (Berlin) have demonstrated <20 ps time resolution [8]. The temporal profile of the field pulse can be measured *in situ* via the chromatic aberration of magnification of the electron optics.

The dynamic response of the domain pattern of a 30 nm thick permalloy ring (o.d. 80 μm, i.d. 37 μm) to the applied field pulse has been investigated. Snapshot domain images have been taken with a temporal increment of 500 ps using a delay element between the field pulse

(pump) and photon pulse (probe). The images reveal the dynamic response being largely dominated by magnetization rotation processes. The given field gradient in the leading edge of the pulse is 1 mT/500 ps; the field amplitude in the plateau is 2 mT. For these conditions the 'slow field' approximation, i.e. a continuous movement of domain walls, cannot describe the remagnetization process. Domain wall motion proceeds at a typical wall speed of a few hundred nanometres per nanosecond. During a field pulse of a few nanoseconds duration, domain walls can move only less than 1 μm. Obviously, this motion cannot substantially change the macroscopic magnetization of elements as large as 80 μm. In this case the system responds by precessional motion of the magnetization. In the trailing edge of the field pulse the negative field gradient of -0.5 mT/500 ps causes the fast formation of a striped domain pattern (incoherent magnetization rotation) penetrating all areas of the ring as well as possibly eddy-current-induced features.

A micromagnetic simulation performed for a smaller permalloy element confirmed the essential dynamical features. In particular the coherent magnetization rotation and the formation of a characteristic pair of antiparallel oriented domains (with their magnetization perpendicular to the field direction) were clearly reproduced. The latter feature occurs in a domain that was initially oriented antiparallel to the external field. The simulation revealed that this behaviour arises only beyond a certain field gradient, i.e. it is a true dynamic feature, being absent in the quasistatic regime or slow field approximation. The observed formation of stripes in the trailing edge of the field pulse was also visible in the simulation. It is connected with residues of vortices at the inner perimeter of the ring persisting during the field pulse. In the trailing edge these vortices act as nucleation centres for the striped pattern. Corresponding simulations for a larger, more realistic element are in progress.

In conclusion, the novel technique of stroboscopic XMCD–PEEM gives direct access to subtle features in the dynamic response of a ferromagnetic domain pattern to a fast magnetic field pulse. The method allows distinguishing between competing processes such as domain wall motion and precessional motion of the magnetization. Transient domain patterns such as the observed onion state can be identified. The relatively large structure studied in the present work shows a complicated multi-domain pattern. A central question will be how the behaviour changes when the size is reduced. The ultimate time resolution in the range of $<$20 ps will give access to the observation of spin waves, domain wall oscillations, magnetic ringing and other phenomena that happen in the frequency domain of several gigahertz. High resolution imaging of the influence of such phenomena on small magnetization structures is of utmost importance for the investigation and optimization of future magnetoelectronic devices.

Acknowledgments

We thank the staff of the ESRF (Grenoble), in particular Nick Brookes and Celine de Nadai, for excellent support and cooperation. Financial support by BMBF (grants 05KS1UM1/5, 05KS1BDA/9, 03N6500 and 13N8269) and by Deutsche Forschungsgemeinschaft through 'Schwerpunktprogramm Ultraschnelle Magnetisierungsprozesse SPP1133' is gratefully acknowledged.

References

[1] Huber A and Schäfer R 1998 *Magnetic Domains* (Berlin: Springer)
[2] Stöhr J, Wu Y, Samant M G, Hermsmeier B D, Harp G, Koranda S, Dunham D and Tonner B P 1993 *Science* **259** 658
[3] Schneider C M and Schönhense G 2002 *Rep. Prog. Phys.* **65** R1785

[4] www.focus-gmbh.com
[5] Krasyuk A, Oelsner A, Nepijko S A, Kuksov A, Schneider C M and Schönhense G 2003 *Appl. Phys.* A **76** 863
[6] Vogel J, Kuch W, Bonfim M, Camarero J, Pennec Y, Offi F, Fukumoto K, Kirschner J, Fontaine A and Pizzine S 2003 *Appl. Phys. Lett.* **82** 2299
[7] Choe S B, Acreman Y, Scholl A, Bauer A, Doran A, Stöhr J and Padmore H A 2004 *Science* **304** 420
[8] Oelsner A, Krasyuk A, Nepijko S A, Kuksov A, Schneider C M and Schönhense G 2003 *BESSY Annual Report* p 329
[9] www.BESSY.de
[10] Feikes J, Holldack K, Kuske P and Wüstefeld G 2003 *BESSY Annual Report* p 520
[11] Nepijko S A, Sedov N N and Schönhense G 2000 Measurement of magnetic fields and domain structures using a photoemission electron microscope *Advances in Imaging and Electron Physics* vol 113, ed P W Hawkes (San Diego, CA: Academic) pp 205–48
[12] Krasyuk A, Oelsner A, Nepijko S A, Sedov N N, Kuksov A, Schneider C M and Schönhense G 2004 *Appl. Phys.* A **79** 1925
[13] Hawkes P W and Kasper E 1996 *Principles of Electron Optics* vol 2 (London: Academic) p 414
[14] Oelsner A, Krasyuk A, Neeb D, Nepijko S A, Kuksov A, Schneider C M and Schönhense G 2004 *J. Electron Spectrosc. Relat. Phenom.* **137–140** 751
[15] Schneider C M, de Haas O, Tietjen D, Muschiol U, Cramer N, Celinski Z, Oelsner A, Klais M, Ziethen Ch, Schmidt O, Schönhense G, Zema N and Zennaro S 2002 *J. Phys. D: Appl. Phys.* **35** 2472
[16] Kläui M, Vaz C A F, Lopez-Diaz L and Bland J A C 2003 *J. Phys.: Condens. Matter* **15** R985
[17] Kläui M, Vaz C A F, Bland J A C, Wernsdorfer W, Faini G, Cambril E and Heyderman L J 2003 *Appl. Phys. Lett.* **83** 105
[18] Porter D G and Donahue M J 2004 *J. Appl. Phys.* **95** 6729
[19] Ruiz-Feal I, Moore T A, Lopez-Diaz L and Bland J A C 2002 *Phys. Rev.* B **65** 054409
[20] Choi B C, Belov M, Hiebert W K, Ballentine G E and Freeman M R 2001 *Phys. Rev. Lett.* **86** 728
[21] Kuksov A, Schneider C M, Oelsner A, Krasyuk A, Neeb D, Schönhense G, de Nadai C and Brookes N B 2004 *J. Appl. Phys.* **95** 6530
[22] Schneider C M, Kuksov A, Krasyuk A, Delsner A, Neeb D, Nepijko S A, Schönhense G, Mönch I, Kaltofen R, Morais J, de Nadai C and Brookes N B 2004 *Appl. Phys. Lett.* **85** 2526
[23] Donahue M J and Porter D G *OOMMF Users's Guide version 1.1b2* National Institute of Standards and Technology (USA) http://math.nist.gov/oommf